Integrated optical SSB modulation / frequency shifting using cascaded silicon MZM

Mehedi Hasan, Omid Jafari, Xun Guan, Leslie A. Rusch, Sophie LaRochelle, and Trevor Hall

IEEE Photonics Technology Letters, (2020)

Doi: 10.1109/LPT.2020.3014221

https://ieeexplore.ieee.org/document/9159677

Integrated optical SSB modulation / frequency shifting using cascaded silicon MZM

Mehedi Hasan, *Student Member, IEEE,* Omid Jafari, Xun Guan, Leslie A. Rusch, *Fellow, IEEE,* Sophie Larochelle, *Senior Member, IEEE* and Trevor Hall, *Senior Member, IEEE*

***Abstract*— A frequency conversion mixer or single side band modulator using two cascaded MZM is proven experimentally. The operation of the circuit is modelled by a transfer matrix approach and verified by simulation in support of the experiment. A 10 GHz shift of the optical carrier in both left and right direction is demonstrated. The residual sideband suppression relative to the enhanced sideband is 22 dB for the best cases. Numerical analysis shows that the circuit has 3-dB optical and 3-dB electrical intrinsic advantage over the functionally equivalent DP-MZM.**

***Index Terms*—MZM, SSB, SSB-SC, Silicon photonics, Photonic integrated circuit.**

I. Introduction

Efficient single side band suppressed carrier (SSB-SC) modulation technology for frequency conversion or shifting is a growing need and fundamental to radio frequency photonic systems. Starting from the very first demonstration [1] of an integrated SSB modulator based on a Ti-diffused $LiNbO_3$ optical waveguide circuit driven by an in-phase (I) and quadrature (Q) signal at 2 GHz, there has been a plethora of publications [2-9] describing different techniques for obtaining the desired functions. All the architectures presented in references [1-5, 7-9] use circuits of Mach-Zehnder Modulators (MZM). Typically, pairs of electro-optic phase modulators are combined to form an MZM. A dual-drive MZM (DD-MZM) is used in [2, 4] to generate the SSB-SC modulation. In this scheme, the optical carrier is modulated by the in-phase and quadrature component of the RF drive signal. However, a dual-parallel Mach Zehnder Modulator (DP-MZM) is the most widely used solution because of its superior carrier and sideband suppression [3,5,7-9]. In this scheme, two child MZM are biased at the minimum transmission point (MITP) while the parent MZM is kept at the quadrature bias point (QTP). Then the I and Q components of the RF signal are applied to the two child MZM. The use of the intrinsic phase relationship between ports of a 1× 3 multimode interference coupler (MMI) has been proposed for selective suppression of unwanted harmonics [6]. A notable advance on the design of the desired function is presented in [7] and a DC bias-less and filter-less scheme based on MMI couplers has been reported [8]. A silicon-based DP-MZM architecture for 1 GHz frequency shifting is reported in [9]. All these architectures are directly equivalent to a single stage generalized Mach-Zehnder Interferometer (GMZI) circuit: an $1 \times N$ splitter directly interconnected to a $N \times 1$ combiner via an array of N linear electro-optic phase modulators. A search for a two-stage cascaded architecture capable of performing SSB was inspired by a publication on frequency multiplication [10]; a cascaded MZM structure requires 3-dB less RF power than the functionally equivalent parallel architecture. Finally, a cascaded MZM architecture capable of performing I-Q and/or SSB modulation with 6-dB intrinsic advantage (3-dB electrical and 3-dB optical) was proposed and verified by simulation in [11]. An alternative implementation based on polarization modulators was reported in [12]. This letter reports the test and measurement of a prototype cascaded MZM architecture on a silicon photonics platform that proves experimentally the proposed architecture and theoretical predictions disclosed in [11]. The three-stage cascaded MZM architecture was designed to be used as an optical digital-to-analog converter for high baud rate PAM transmission. It was fabricated on the same multi project wafer (MPW) run, and with the same RF transmission line design, as the single MZM with segmented electrodes in [13]. The details of the fabrication technology of the silicon photonic chip and

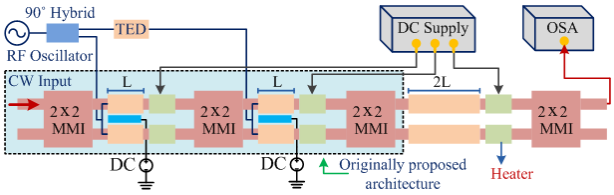

Fig. 1. Schematic diagram of the photonic integrated circuit architecture and experimental arrangement; OSA, optical spectrum analyzer; TED, tunable electrical delay; DC, direct current; CW, continuous wave.

This paragraph of the first footnote will contain the date on which you submitted your paper for review. It will also contain support information, including sponsor and financial support acknowledgment.

Mehedi Hasan and Trevor Hall are with Photonic Technology Lab (PTL), University of Ottawa, 25 Templeton St, Ottawa, K1N 6X1, ON, Canada.(e:mail: mhasa067@uottawa.ca; trevor.hall@uottawa.ca). Omid Jafari, Xun Guan, Leslie A. Rusch and Sophie Larochelle are with Centre d'optique, photonique et laser (COPL), Université Laval, 2375 rue de la Terrasse, Québec QC, Canada, G1V 0A6 (e-mail : sophie.larochelle@gel.ulaval.ca).

National Science and Engineering Research Council of Canada (NSERC) Funding: CRDPJ 438811-12

the electrode electro-optic (E/O) characterization can be found in [13]. Ideally, the present demonstration of SSB generation would have required a two-stage cascaded MZ structure. Consequently, the three stage MZM, readily available in our laboratory, was adapted for this application by appropriate tuning of the exit stage.

II. Principal of Operation

Fig. 1 shows the schematic of the fabricated circuit architecture used for the experimental verification. The originally proposed circuit architecture consisting of two cascaded MZM is highlighted in the schematic. It can be seen that the original architecture is identical to the fabricated chip except for the last stage MMI. The novelty of the circuit architecture is the coupling between the two MZM used. A 2×2 MMI is used as the exit coupler of the 1st MZM and entrance coupler for the 2nd stage MZM. Thereby creating special coupling and phase bias. Since there is no unused port between the stages, the optical insertion loss is reduced by 3 dB from the orthodox arrangements given that the phase modulators are lossless (or negligible loss) and equal in length for both cascade and parallel cases. For lossy modulators, the optical advantage will be reduced by the attenuation of the additional stage. However, the architecture has less intrinsic loss due to reduced (halved) number of splitters and combiners. An additional 90° optical phase shift is required in both the stages for the target application. Each light path is modulated twice (1st stage & 2nd stage) in this architecture, so the RF power required to achieve a specified phase modulation magnitude is 3-dB less than the RF power required for the same phase modulation by a parallel MZM architecture, which modulates each light path only once. Hence, the proposed circuit is 6-dB (3-dB optical and 3-dB electrical) advantageous in principle.

To implement the same function using the three stage MZM, the 90° optical phase bias is applied in the 3rd stage instead of the 2nd stage as in the original design. The in-phase and quadrature-phase RF signal is applied to the 1st stage and 2nd stage respectively. The 2×2 MMI present in the fabricated chip are identical in design as in [14]. A thermo-optic phase shifter is present in each of the arms between stages. The modulator was fabricated at IME A*star on the same run and with the same electrode design as the segmented MZM in [13]. The phase-shifter length of the first two stages is L=1500 μm and 2L=3000 μm for the third stage, for a total phase shifter length of 6 mm (compared to 3.5 mm in [13]). The MZM is designed to be driven in a push-pull (PP) configuration. A 50 Ω termination is used in the MZM for impedance matching with the RF drivers. Deep UV photolithography is used to fabricate the modulator. The BOX thickness was 3μm, whereas a top-silicon layer of 200 nm was used in the wafer. The width of the modulator ridge waveguide is 500 nm; whereas slab thickness is 90 nm [13]. Figure 2 shows the E/O characterization of the modulator with a length of 2000 μm. The 3-dB bandwidth of the modulator is found to be ∼38 GHz. However, the bandwidth of the 1500 μm phase shifter will be greater than 38 GHz due to low microwave loss and reduced velocity mismatch between the optical and electrical wave.

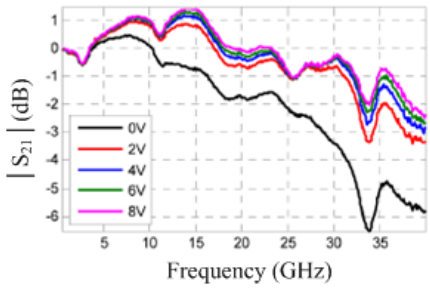

Fig. 2. Normalized E/O $|S_{21}|$ for 2000 μm long phase shifter with reverse bias voltages from 0 to 8 V. Adapted with permission from [1] © The Optical Society.

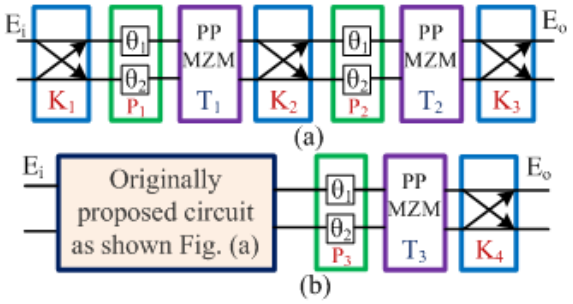

Fig. 3. Functional diagram; (a) originally proposed circuit; (b) circuit adopted for experimental demonstration; PP, push-pull.

Neglecting the propagation delay between the stages the functional diagram (Fig. 3) may be represented by transfer matrices. The output of the originally proposed circuit can be written:

$$E_o = \frac{1}{2\sqrt{2}} K_3 P_2 T_2 K_2 T_1 P_1 K_1 E_i \tag{1}$$

where:

$$K_j = \frac{1}{\sqrt{2}} \begin{bmatrix} 1 & -i \\ -i & 1 \end{bmatrix}$$

describes a 2× 2 MMI; and P_1, P_2 describe the static optical phase shifts applied in the 1st & 2nd stage MZM, respectively. Here, E_i and E_o are 2×1 column vectors. The choice of input and output port is determines which of their two elements is chosen as non-zero. Given an upper port input for upper sideband (USB) or lower sideband (LSB) modulation with upper (UEP) or lower (LEP) exit port:

$$P_1 = \begin{bmatrix} i & 0 \\ 0 & 1 \end{bmatrix} (USB) \quad ; \quad P_1 = \begin{bmatrix} 1 & 0 \\ 0 & i \end{bmatrix} (LSB)$$
$$P_2 = \begin{bmatrix} i & 0 \\ 0 & 1 \end{bmatrix} (UEP) \quad ; \quad P_2 = \begin{bmatrix} 1 & 0 \\ 0 & i \end{bmatrix} (LEP)$$

and:

$$T_1 = \begin{bmatrix} e^{i\varphi_1} & 0 \\ 0 & e^{-i\varphi_1} \end{bmatrix} \quad \& \quad T_2 = \begin{bmatrix} e^{i\varphi_2} & 0 \\ 0 & e^{-i\varphi_2} \end{bmatrix}$$

describe the 1st & 2nd stage optical phase modulators. Here:

$$\varphi_j = \pi \, v_j / v_\pi \tag{2}$$

is the optical phase shift induced by the RF signal v_j and v_π is the half-wave voltage of the phase modulators. Simplifying (1) gives:

$$E_0 = \left(1/\sqrt{2}\right) i [\sin(\varphi_1 + \varphi_2) + i \sin(\varphi_1 - \varphi_2)] E_i \tag{3}$$

National Science and Engineering Research Council of Canada (NSERC) Funding: CRDPJ 438811-12

Setting:

$$v_1 = v_Q \quad \& \quad v_2 = v_I \tag{4}$$

then for $|v_I|, |v_Q| \ll v_\pi$

$$E_0/E_i = (\pi/v_\pi)\left(v_I + i v_Q\right)\exp(i\,\pi/4) \tag{5}$$

demonstrating that circuit performs I-Q modulation.

The implementation of the same function using a three-stage cascaded MZM is not as straight forward as described in the preceding. The second stage optical phase shift is applied in the 3rd stage to ensure the quadrature operation of the final stage MZM. On the other hand, the I and Q signals are applied in the 1st stage and 2nd stage MZM as per the originally proposed architecture. The total transmission may be written as:

$$E_o/E_i = (1/4)K_4P_3K_3T_2K_2T_1P_1K_1 \tag{6}$$

where P_1,P_2 are chosen as before. Equation (6) simplifies to:

$$E_0/E_i = (1/2)i[\sin(\varphi_1 + \varphi_2) + i\sin(\varphi_1 - \varphi_2)] \tag{7}$$

Equation (7) is identical to (3) except for the reduction of the optical amplitude by a factor of $1/\sqrt{2}$ due to the redundant 3rd stage of the photonic integrated circuit used. In the case of an applied RF-signal of the form:

$$v_1(t) = v_{RF}\cos(\omega t) \quad \& \quad v_2(t) = v_{RF}\sin(\omega t) \tag{8}$$

The circuit provides lower sideband modulation or frequency down conversion. By interchanging the drive signals, one can obtain frequency up-conversion or upper side band modulation. Hence, the circuit works as electro-optic up/down conversion mixer or frequency shifter. Invoking the Jacobi Anger expansion, Eq. (7) may be rewritten:

$$E_0/E_i = \sum_{n=0}^{\infty}(-1)^n J_{2n+1}(m)\exp\left[i(-1)^n(2n-1)\left(\omega t - \frac{\pi}{4}\right)\right] \tag{9}$$

where, J_ν is the Bessel function of the first kind of order ν and

$$m = \sqrt{2}\pi\, v_{RF}/v_\pi \tag{10}$$

is the modulation index. The pre-factor $\sqrt{2}$ confirms the 3-dB electrical advantage of the proposed architecture in comparison to circuits presented in [5, 8-9]. The 3-dB optical advantage is not realised because of the presence of the third stage. However, the original design confirms the 3-dB optical advantage as well. It can be understood from (9), that all the even harmonics are suppressed including the carrier. The principal sidebands are -1, +3, and -5.

III. Result

The circuit architecture proposed is validated by the industry-standard software tool (VPIphotonics™) and laboratory experiment. In the simulations, a 1540 nm CW-DFB laser having power of 0 dBm is used as the optical input. All the MMIs are configured to have more than 1˚ phase error and 1% power imbalances. A 10 GHz RF source having peak amplitude of $v_{RF} = 0.1v_\pi$ V (m~0.44 as per (10)) and appropriate phase shift is chosen to emulate the experiment. Fig. 4 shows the simulated optical spectrum of the frequency shift operation. In

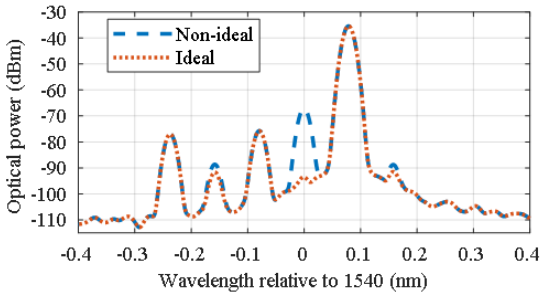

Fig. 4. Simulated optical spectrum; Ideal, refers to the exact optical phase shift between the stages and Non-ideal represent slight detuning from the ideal. The optical noise floor is determined by the laser linewidth.

the laboratory experiment, the coupling and on-chip loss is found to be 25 dB (~16 dB coupling loss and ~9 dB on-chip loss). The 9 dB on-chip loss is in agreement with the loss value (5 dB) reported in [13] considering the longer phase shifters and routing waveguides, and the presence of two additional MMI. However, the coupling loss is 4 dB higher (16 dB vs 12 dB) due to a non-optimum fiber array. Hence, a 25-dB attenuator is used in the simulated circuit to account for the coupling and on-chip loss. Note that state-of-the-art silicon photonic modulators can be designed with lower than 1 dB of coupling loss using edge couplers [15], subwavelength gratings [16], or photonic wire bonding [17].

The theoretical analysis of the circuit architecture is relatively straightforward; however, achieving the correct quiescent operating point experimentally is complicated by imbalance of the optical path lengths in the different stages of the test architecture and other impairments due to fabrication errors. Nevertheless, thermo-optic phase shifters are present in every stage for appropriate phase tuning. Firstly, a DC characterization was performed with the assistance of the algorithm presented by Wilkes et al [18]. Using the algorithm, the extinction ratio at the upper output port is maximized to greater than 40 dB. The lower port extinction is improved similarly. The algorithm works on the principle that the first stage MZI acts as a variable beam splitter and the last stage MZI acts as a variable beam combiner while the complete circuit acts as a single MZI controlled by the phase shifters in the central stage. The high extinction at the upper output port ensures that the complete circuit acts as an ideal MZI; when the second stage phase shifter is adjusted to maximized transmission, the optical input to the upper input port exits only from the upper output port. Following the achievement of this bias state an additional 90˚ optical phase bias is applied at the 1st stage and 3rd stage to achieve the correct bias state for single sideband modulation. A fine tuning of the bias voltages is required for proper operation. A laser source providing 0 dBm power at a vacuum wavelength of 1540.01 nm was used as the optical input. An Anritsu 3695C RF signal generator was used as RF signal source. A 10 GHz sinusoid having power of 18 dBm was used as the analog RF input to the circuit. A 90˚ RF hybrid coupler from Krytar (model 3014320; 1.4-32 GHz) was used to create the in-phase (I) and quadrature-phase (Q) channels. The insertion loss of the hybrid is about 3.5 dB, while the amplitude imbalances and phase

National Science and Engineering Research Council of Canada (NSERC) Funding: CRDPJ 438811-12

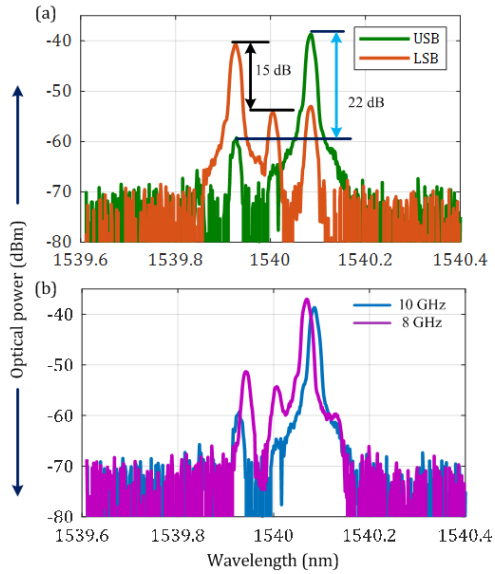

Fig. 5. Measured optical spectra for (a) upper side band (USB) and lower side band modulation (LSB); (b) upper side band modulation for two different RF frequency. A resolution bandwidth of 0.02 nm is used for measurement.

imbalances are ± 1.55 dB and $\pm 12^{\circ}$ respectively. A mechanical phase shifter from API technologies (OPS -0002) was used in one of the arms at the output of the hybrid coupler for fine tuning of the phase of the RF signal. The insertion loss of the device was 3-5 dB. Finally, the RF signal was applied to the RF pad of the circuit using a RF probe. The RF coaxial cable connected between the RF probe and the 90° hybrid added a further 2-3 dB of loss. Fig. 5 (a) shows the measured frequency down-conversion (green) from the upper output port. The bias voltages at the thermo-optic phase shifters are 5.10 V, -3.24 V and 3.20 V for the 1st stage, 2nd stage and 3rd stage respectively. The optical spectra show that a side harmonic suppression ratio of more than 20 dB can be obtained by fine tuning of the bias voltages. Frequency up- conversion (orange) is obtained from the same output port when the input optical signal is changed from upper input port to the lower input port. For the identical bias voltages, the side harmonic suppression is reduced to some extent from the previous case. The modulation index is ~ 0.35-0.40, far from the peak ($m =\sim 2$) of the first harmonics. A low v_{π} modulator can be used to improve the conversion efficiency. Fig. 5 (b) shows the output optical spectra for 10 GHz and 8 GHz RF signal. Since the chip was not wire bonded, and there is no heat sink to stabilize the temperature, slight variation in the optical spectra were observed due to thermal drift of the bias point. Nevertheless, a side harmonic suppression ratio of 15 dB or more is obtained in all cases.

IV. Conclusion

In summary, the experimental verification of a previously proposed two stage cascaded circuit architecture for single side band modulation was performed. A three-stage cascaded circuit architecture fabricated for high baud rate PAM transmission was adapted for the experimental demonstration. The experimental result shows that, the circuit can perform SSB modulation with a side harmonic suppression ratio of at least 15 dB or more. Careful design and experiment are required to improve the performance further. However, it is now proven that a two-stage cascaded MZM can be used for SSB and/or I-Q or complex modulation with greater energy efficiency. The device was fabricated using CMOS compatible silicon photonics technology.

Acknowledgment

The authors acknowledge Dr Alexandre D. Simard for the cascaded MZM design. Device fabrication was made possible with the help of TeraXion, CMC Microsystems and NSERC through CRD project grant 438811-12.

References

[1] M. Izutsu, S. Shikama, T. Sueta, 'Integrated optical SSB modulator / frequency shifter', 'IEEE J. Quantum Electron., vol. 17, no. 11, pp. 2225-2227, Nov. 1981.
[2] G. H. Smith, D. Novak, and Z. Ahmed, "Overcoming chromatic-dispersion effects in fiber-wireless systems incorporating external modulators," IEEE Trans. Microw. Theory Tech., vol. 45, no. 8, pp. 1410-1415, Aug. 1997.
[3] S. Shimotsu et al., Single side-band modulation performance of a LiNbO3 integrated modulator consisting of four-phase modulator waveguides," IEEE Photon. Technol. Lett., vol. 13, no. 4, pp. 364-366, Apr. 2001.
[4] J. Yu, Z. Jia, L. Yi, Y. Su, G.-K. Chang, and T. Wang, "Optical millimeter-wave generation or up-conversion using external modulators," IEEE Photon. Technol. Lett., vol.18, no. 1, pp.265-267, Jan. 2006.
[5] C. W. Chow, C. H. Wang, C. H. Yeh, and S. Chi, "Analysis of the carrier-suppressed single-sideband modulators used to mitigate Rayleigh backscattering in carrier-distributed PON" Opt. Express, vol. 19, no. 11, pp. 10973-10978, May 2011.
[6] J.-G. Zhao, Z. J. Liu, X.-L. Liu, T. Shang, and P. Yue, "Optimisation of carrier-to-sideband ratio by triple-arm Mach-Zehnder modulators in radio-over-fibre links," IET Optoelectron., vol. 4, no. 5, 183-188, Oct. 2010.
[7] M. Hasan, R. Maldonado-Basilio, and T. J. Hall, "A dual-function photonic integrated circuit for frequency octo-tupling or single-side-band modulation" Opt. Lett., vol. 40, no. 11, pp. 2501-2504, May 2015.
[8] R. Maldonado-Basilio et al., Electro optic up-conversion mixer amenable to photonic integration," J. Mod. Opt., vol. 62, no. 17, pp.1405-1411, May 2015.
[9] Kodigala et al., Silicon Photonic Single-Sideband Generation with Dual-Parallel Mach-Zehnder Modulators," in Proc. CLEO, San Jose, CA, USA, 2019.
[10] M. Hasan, T. J. Hall, "A photonic frequency octo-tupler with reduced RF drive power and extended spurious sideband suppression," Opt. Laser Technol., vol. 81, pp. 115-121, Jul. 2016.
[11] M. Hasan and T. Hall, "Cascade photonic integrated circuit architecture for electro-optic in-phase quadrature/single sideband modulation or frequency conversion," Opt. Lett., vol. 40, no. 21, pp. 5038-5041, Sep. 2015.
[12] M. Hasan and T. Hall, "Complex modulation using tandem polarization modulators," J. M. Opt., vol.64, no. 20, pp. 2268-2272, Jun 2017.
[13] A. Simard, B. Filion, D. Patel, D. Plant, and S. LaRochelle, "Segmented silicon MZM for PAM-8 transmissions at 114 Gb/s with binary signaling," Opt. Express, vol. 24, no. 17, pp. 19467-19472, Aug. 2016.
[14] A. Simard and S. LaRochelle, "Complex apodized Bragg grating filters without circulators in silicon-on-insulator," Opt. Express, vol. 23, no. 13, pp. 16662-16675, Jun. 2015.
[15] T. Tsuchizawa et al., Microphotonics devices based on silicon microfabrication technology," IEEE J. Sel. Top. Quantum Electron., vol. 11, no. 1, pp. 232-240, Feb. 2005.
[16] P. Cheben et al., Refractive index engineering with subwavelength gratings for efficient microphotonic couplers and planar waveguide multiplexers," Opt. Lett., vol. 35, no. 15, pp. 2526-2528, Jul. 2010.
[17] N. Lindenmann et al., Photonic wire bonding: a novel concept for chip-scale interconnects," Opt. Express, vol. 20, no. 16, pp. 17667-17677, Jul. 2012.
[18] C. Wilkes et al.,60 dB high-extinction auto-configured Mach–Zehnder interferometer," Opt. Lett., vol. 41, no. 22, pp. 5318-5321, Nov. 2016.

National Science and Engineering Research Council of Canada (NSERC) Funding: CRDPJ 438811-12